JOURNAL OF GEOPHYSICAL RESEARCH, VOL. 100, NO. B7, PAGES 12,375–12,394, JULY 10, 1995

A global tomographic model of shear attenuation in the upper mantle

B. Romanowicz

Seismographic Station and Department of Geology and Geophysics, University of California, Berkeley

Abstract. We present a global three-dimensional model of shear attenuation in the upper mantle, based on the measurement of amplitudes of low-frequency (100-300s) Rayleigh waves observed at stations of the Geoscope and Iris networks. Attenuation coefficients are measured on R1 and R2 paths using a method which minimizes the effects of focussing due to propagation in a three-dimensional elastic Earth. Through a series of tests which, in particular, involve the computation of synthetic models of attenuation and focussing, we demonstrate that long wavelength lateral variations in attenuation in the first 400-500 km of the mantle can indeed be resolved. The model is obtained in a two-step procedure. The first step consists in the computation of maps of Rayleigh wave attenuation at different periods, using an inversion method without a priori parametrisation, which involves the introduction of a correlation length, chosen here at 3000 km to optimize the trade-off between resolution and variance in the model. In the second step, after corrections for shallow structure, an inversion with depth is performed, assuming lateral heterogeneity is confined to depths between 80 and 650 km. The resulting model presents lateral variations in Q_β that are correlated with tectonic features, in particular ridges and shields in the first 250 km of the upper mantle. Below that depth the pattern shifts and becomes correlated with the hotspot distribution, particularly so if the buoyancy strength of hotspots is taken into account. Two major low-velocity zones appear to be located in the central pacific and beneath northern Africa, in the depth range 300-500 km. This pattern seems to continue at greater depth, but resolution becomes insufficient below 500 km to draw definitive conclusions. The smooth lateral variations retrieved are on the order of ±50% down to 400 km. We propose an interpretation in terms of plume/lithosphere/ridge interaction in the upper mantle, arguing for deflection of the bulk of hot upwelling material from plumes towards ridges, which may be occurring between 200 and 300 km depth.

Introduction

Global three-dimensional (3D) anelastic structure of the Earth's mantle remains poorly resolved by comparison with elastic structure, although evidence for large lateral variations in upper-mantle Q has been abundant since the 1970s. Measurements of Q_{ScS} from multiple bouncing ScS_n waves have shown large differences between ocean basins, subduction zones, and back arc regions [*Sipkin and Jordan*, 1980; *Nakanishi*, 1979; *Lay and Wallace*, 1983; *Chan and Der*, 1988; *Flanaghan and Wiens*, 1990]. Fundamental mode free oscillation and low frequency mantle wave studies have documented lateral variations in excess of ±50% and interpreted them in the context of simple regionalized models according to tectonic provinces [e.g., *Mills and Hales*, 1978; *Nakanishi*, 1978; *Roult*, 1982; *Dziewonski and Steim*, 1983]. Crustal Q has been extensively studied using short-period surface waves, also showing strong dependence on tectonic environment [e.g., *Mitchell*, 1975; *Yacoub and Mitchell*, 1977; *Canas and Mitchell*, 1978]. At the regional scale, high attenuation has been recently documented near ridges [e.g., *Sheehan and Solomon*, 1992; *Ding and Grand*, 1993; *Bussy et al.*, 1993].

Yet few attempts have been made at tomographic modelling of Q on the global scale, and, so far, lateral variations in mantle wave and free-oscillation Q have been mostly described in terms of maps of quality factors for Rayleigh and Love waves, $Q_R(\omega)$ and $Q_L(\omega)$ respectively, at selected periods, often limited to even degrees, that is features symmetric with respect to the center of the Earth [*Romanowicz et al.*, 1987; *Roult et al.*, 1990; *Suda et al.*, 1991; *Smith and Masters*, 1989; *Durek et al.*, 1993]. The depth dependence, on the other hand, has only been discussed very cautiously: *Romanowicz* [1990] only inverted for the depth dependence of degree 2 in shear attenuation, $Q\mu^{-1}$, while *Durek et al.* [1993] considered a single layer inversion for even orders up to degree 6.

Paper number 95JB00957.
0148-0227/95/95JB-00957$05.00

There are at least two reasons why the aneastic structure of the mantle should be of fundamental interest to geophysicists. First, absorption may be band-limited within the seismic frequency band, with a possible high-frequency cutoff located roughly between 1 and 10 s, as inferred from seismic observations [e.g., *Sipkin and Jordan*, 1979], and this may have important consequences on the comparison of models obtained using waves of different frequencies (such as models based on short-period body waves on the one hand, and models based on waveform modelling of low frequency waves, on the other) because of physical dispersion effects [e.g.,*Liu et al.*, 1976; *Minster and Anderson*, 1981]. Anelastic structure also needs to be considered when comparing different geophysical observables, such as seismic velocities and the geoid [e.g., *Hager et al.*, 1985; *Ricard et al.*, 1993; *Forte et al.*, 1994], for which it is generally assumed that the conversion coefficient between velocities and densities does not vary spatially [*Karato*, 1993].

The other important reason for considering 3D anelastic structure is that it may provide constraints on mantle dynamics that are complementary to those inferred from elastic modeling. Indeed, if, as thought to be the case, the dominant contribution to absorption of seismic waves in the mantle is due to thermally activated mechanisms, the temperature dependence of Q follows an Arrhenius exponential law and is therefore much stronger than that of elastic velocity [e.g., *Minster and Anderson*, 1981; *Kampfman and Berckhemer*, 1985; *Jackson et al.*, 1992]. In Figure 1, we present a sketch illustrating how this difference in behavior of elastic velocities and Q with temperature might reflect itself in tomographic maps: "weak" upwelling currents of elevated temperature relative to the surroundings can be emphasized through the mapping of Q^{-1}, whereas they are hard to detect in the presence of "strong" cold downwellings (such as slabs in the upper mantle) when mapping elastic velocities. Recent global elastic tomographic models have had more success in recognizing coherent fast-velocity structures in the upper mantle and top of the lower mantle, associated with slabs than features that might be unequivocally associated with hot upwelling currents, and this tends to support geodynamic models where cold downwellings provide the principal driving mechanism of convective motions in the mantle [e.g., *Tackley et al.*, 1993; *Solheim and Peltier*, 1994]. The question of shape, size and original depth of hot upwellings remains open [e.g., *Hansen et al.*, 1993].

The main reason for the present lack of tomographic Q models is the extreme difficulty of extracting reliable attenuation information from the measurement of amplitudes of seismic waves. Indeed, in addition to anelastic attenuation, amplitudes are sensitive to effects due to 3D elastic structure, which create focussing/defocussing of energy [e.g. *Resovsky and Ritzwoller*, 1994], and, at higher frequencies, scattering. The relative contributions of elastic and anelastic effects can be of the same order of magnitude, in the presence of strong gradients in the elastic structure. Present 3D models of elastic velocities are not accurate enough, as

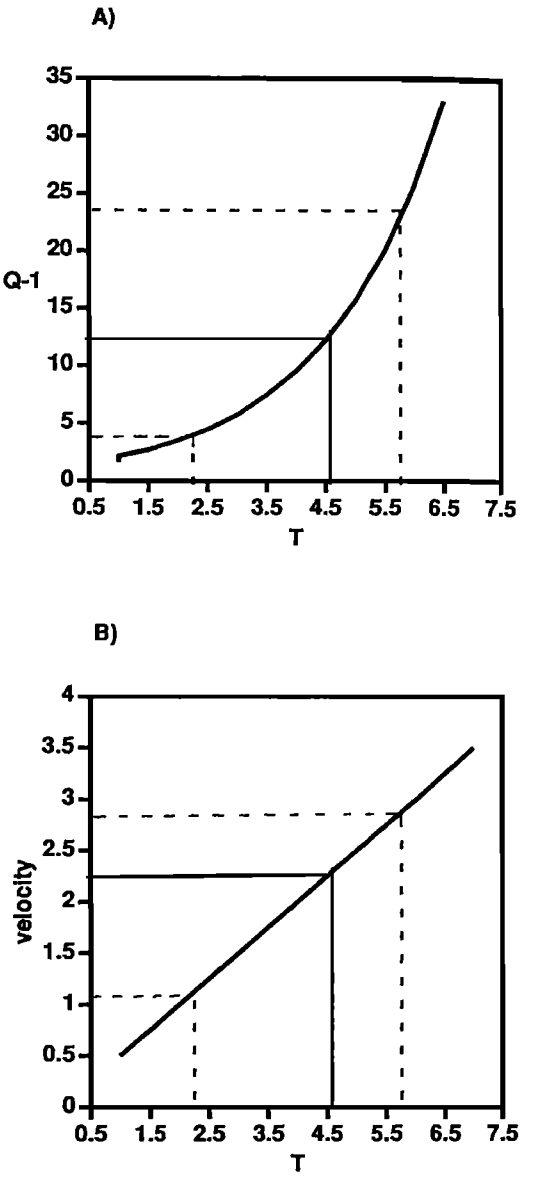

Figure 1. Sketch illustrating the different effects of temperature anomalies on Q and elastic velocity. Units are arbitrary. The temperature anomalies are referred to an average value near $T = 4.5$. (a) The exponential dependence of Q^{-1} on temperature favors hotter than average anomalies, even if colder than average anomalies have larger amplitude. (b) The more linear dependence of elastic velocity on temperature will emphasize the anomalies that are larger in amplitude, that is, "cold" anomalies.

we will illustrate below, to allow the correction of amplitude data by forward modelling of elastic effects.On the other hand, ignoring the latter completely is not possible, since they may create biases that will dominate the resulting tomographic maps. Previous attempts at dealing with focussing effects have relied on the fact that, in the linear approximation [*Woodhouse and Wong*, 1986; *Romanowicz*, 1987; *Park*, 1987], four consecutive surface wave trains can be combined to cancel out these effects [*Romanowicz*, 1990; *Durek et al.*, 1993], a procedure called "desensitizing" by *Durek et al.* [1993]. This

procedure, however, limits the period range of analysis and the size of events considered, since the signal to noise ratio has to be good through at least the fourth wave train (R4, G4). Also, the longer the wave path, the less valid the linear approximation.

In what follows, we present the results of a global tomographic inversion for lateral variations in $Q\mu$ in the upper mantle, using a dataset of Rayleigh wave attenuation coefficients in the period range 100-300 s. The measurement method has been designed so as to minimize biases due to focussing and is described in detail in a separate publication [*Romanowicz*, 1994a, hereafter referred to as paper].

We first review the philosophy and the main characteristics of the measurement method, describe the dataset and the tomographic inversion procedure, and present the resulting 3D model. We then discuss in depth the issue of biases due to focussing effects and establish which features of the 3D model can be considered as reliable. Finally, we discuss geodynamic implications of our results.

Data Collection, Measurement and Inversion Procedures

The data used are fundamental mode Rayleigh wave trains extracted from very long period vertical component seismograms recorded at stations of the global Geoscope network for the time period 1987-1992 [*Romanowicz et al.*, 1991] and GSN of IRIS (Global Seismic Network of the Incorporated Research Institutions for Seismology) for the time period 1990-1992. Events of surface wave magnitude greater than $Ms6.7$ are considered and a severe data selection is performed.

First, only those records are kept which correspond to lobes in the Rayleigh wave radiation pattern, as determined from the published Harvard centroid moment tensor solutions [CMT, *Dziewonski et al.*, 1981]. This first selection is based on the observation that off-path and other "perturbing" effects, which we are trying to avoid, are, in general, much stronger at near-nodal stations.

Further data selection occurs during the measurement process. For each seismogram, the first three Rayleigh wave trains (R1, R2, R3) are windowed with appropriate group velocity windows to avoid contamination by higher modes and overlapping trains, for a period range between 80 and 320 s. As described in paper 1, attenuation coefficients are then measured successively for R1 and R2 paths using, for each, two different methods: (1) a combination of consecutive trains, including R3, whereby the effect of the source (which may not always be perfectly modelled using the CMT solution) is eliminated; and (2) using only R1 (or only R2) and assuming the source amplitude is that given by the CMT solution. The measurement obtained using method (2) is adjusted, through the introduction of a linear "shift", to coincide, inasmuch as possible, over a sufficient period range (80 s or more) with the measurement obtained using method (1). Measurements obtained using method (1) often present large band-limited structures, which are not coherent over neighboring paths and are therefore likely to be due to strong elastic effects, or other non Q related perturbations. We only keep those measurements for which the results of both method (1) and method (2) are smooth as a function of frequency and have shapes that can be well superposed. This leads us to sometimes reject a complete record or keep only R1 or only R2. Moreover, if the shift measured as mentioned above is due to an adjustment in the seismic moment and source mechanism with respect to the CMT solution, it should be the same whether the procedure is applied to R1 or to R2. We therefore reject records for which the two shifts differ by more than 10%, which indicates either directivity of the source, or, more likely, strong focussing effects on either path. Figure 2 shows one example of measurement kept and one rejected, other examples can be found in paper 1. This procedure results in a severe reduction of the total dataset kept for the inversion. Out of over 2000 measurements (R1 and R2), our final data set dwindled to 722, or about one third of the original data at this stage.

To further eliminate outliers, we then calculate, at each period, the average attenuation coefficient, for R1 and R2 trains separately, and keep only those data which do not exceed the average over the whole data set, in absolute value, by 80% and 40% respectively, taking into account the greater smoothing expected for R2 trains, which travel on average three times farther than R1 trains. This imposes a conservative upper limit on the retrieved lateral variations in Q. Further discussion of this method can be found in paper 1.

This very strict data selection allows us to eliminate paths contaminated strongly by band-limited focussing effects. Clearly, it does not necessarily free us of "smooth" focussing effects that might be of the same order of magnitude as attenuation effects and remain undetected because of their smooth variation in frequency. Since such effects are due primarily to smooth, low-degree features of the elastic structure, they can be realistically estimated using existing elastic 3D models of the Earth. In what follows, we will present a series of tests which indicate that, whereas our final data set may still contain smooth focussing effects, these do not impact the resulting 3D anelastic model significantly.

An important point to address before the inversion is, as for elastic tomography, that of crustal corrections: the low-frequency waves used in the inversion have little resolution in the first 50 km below the surface, yet the strong lateral variations of structure in this depth range may bias the derived models [*Woodhouse and Dziewonski*, 1984; *Montagner and Tanimoto*, 1991]. I have considered a simple "shallow layer" model for Q, based on the results of regional short period surface wave studies [*Mitchell*, 1975; *Mitchell et al.*, 1977; *Yacoub and Mitchell*, 1977; *Canas and Mitchell*, 1978] and the regionalization of *Jordan* [1981], where orogenic and phanerozoic zones have been pulled together, resulting in five distinct regions (three oceanic, according to

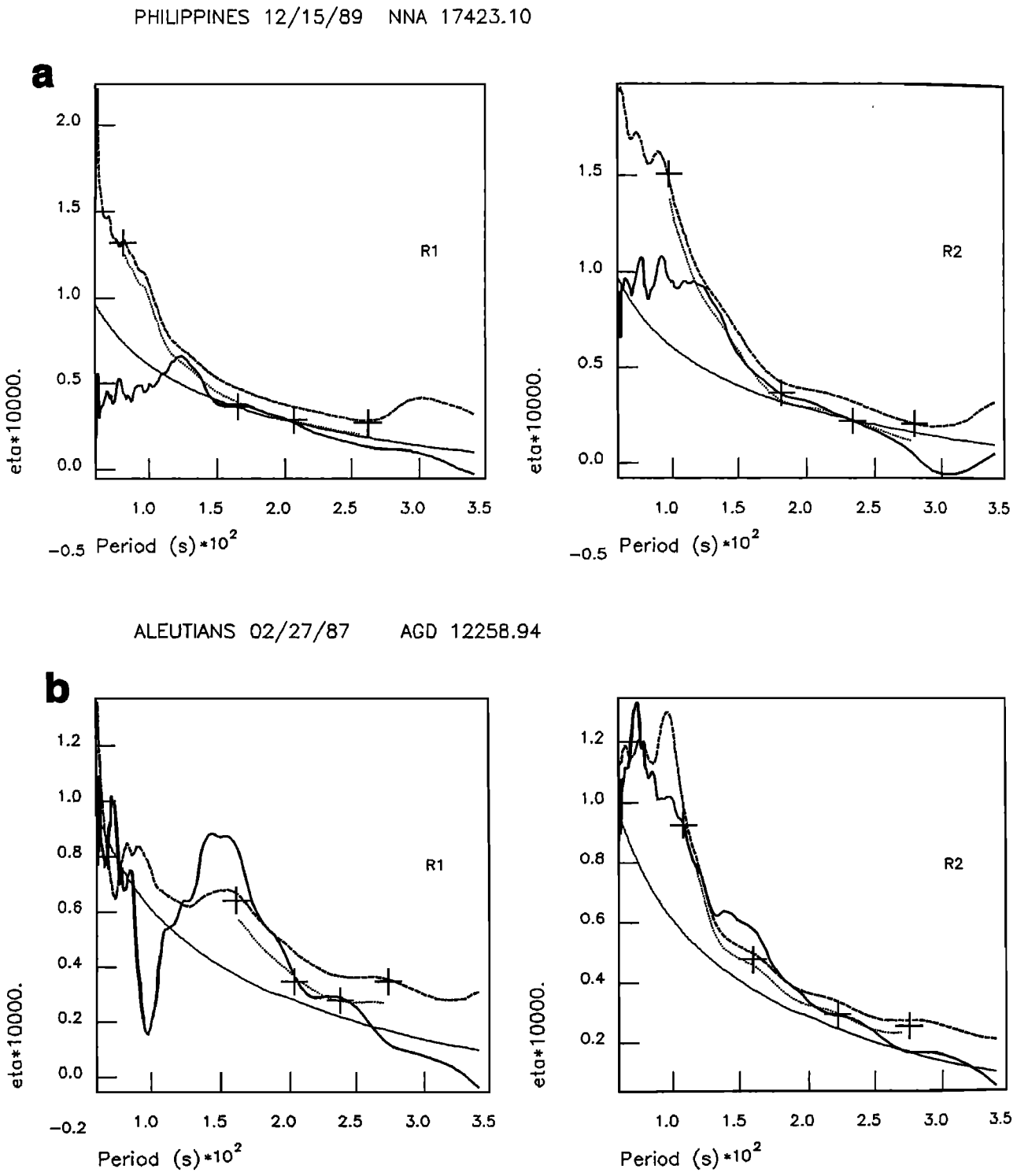

Figure 2. (a) Example of "successful" measurement of attenuation coefficient (eta) on both R1 (left) and R2 (right) wave trains for an event in the Philippines observed at IRIS station NNA. The dashed line represents the original measurement obtained using R1 only (method 2 in text), and the dotted line, the final measurement after applying a constant shift to align with the measurement obtained using R1R2R3 (method 1, solid line). The thin solid line corresponds to the reference PREM model [*Dziewonski and Anderson*, 1981]. The thick crosses indicate the period interval for which the final measurement is kept, and the thin crosses, the period interval over which the shift between results using methods 1 and 2 is calculated. (b) Same as (a) for a path which has been rejected because of spectral holes and lack of agreement between measurements using methods 1 and 2.

age; two continental: tectonic and stable). The crustal contribution to attenuation measurements on individual source-station paths is substracted from the data before inversion. The effect is to decrease the lateral variations in the first 250 km by less than 10% .

The inversion then proceeds in two steps, following the classical approach used for single mode surface wave data in the frequency domain: first, obtain maps of local attenuation at given periods, second, invert for depth dependence. In the first step we apply a tomographic method based on the formalism of *Tarantola and Valette*[1982], as adapted to surface waves by *Montagner* [1986]. This method does not require the expansion of lateral heterogeneity into a specific set of basis functions, such as spherical harmonics, and thereby avoids problems due to truncation. It relies on the construction of a covariance function between couples of paths, which is computed by introducing a correlation length, whose value is adapted to the particular distribution of paths, in order to optimize the question of resolution versus variance present here as in all inverse problems. This method has the added advantage of weighting the data in such a way as to compensate for the non uniform distribution of paths over the sphere, thus limiting biases due to concentrations of paths over specific regions of the Earth. The correlation length chosen here is 3000 km, yielding a model which can resolve the same kind of details as a spherical harmonics expansion of degree 6 to 7.

In this first step of the inversion, two iterations are performed at each period, rejecting, in the second iteration, those paths which yielded residuals greater than 15% in the first iteration. We assume 15% error in the data, based on typical standard deviations computed for paths for which at least four independent measurements are available. This conservative error accounts for the fact that the amplitude measurements contain elastic effects that will not be modelled. Maps of Q^{-1} are obtained at different periods between 80 and 320 s ; those at periods of 284, 269, 256, 232, 213, 200, 182, 170, 160, 150, 140, 134, 128, and 120 s are selected for the second step of the inversion, and corresponding error maps are simultaneously computed. At periods longer than 300 s and shorter than 120 s, data coverage is insufficient to allow further 3D analysis. The variance reduction obtained after the first iteration is typically on the order of 60%. A subset of these maps is presented in paper 1. In Figure 3 we present, for comparison with other recent studies, the symmetric parts, with respect to the center of the Earth, of maps at 232 s and 160 s. We

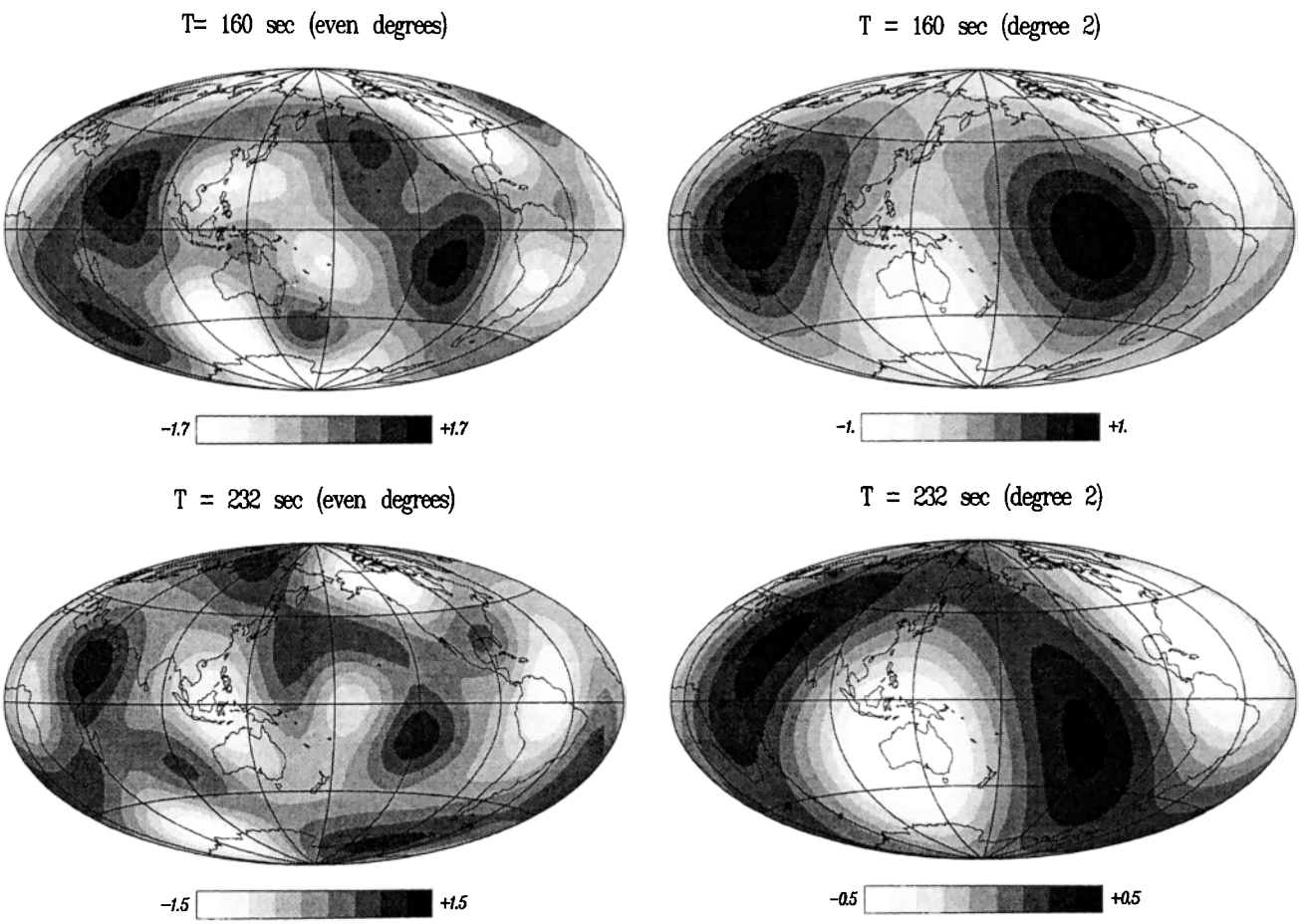

Figure 3. (left) Even degree maps extracted from the results of step 1 of the inversion at periods of 160 s and 232 s. (right) Corresponding degree 2 maps. Perturbations in Q^{-1} with respect to average are presented. Average is $Q^{-1} = 8.1 \times 10^{-3}$ at 160 s and $Q^{-1} = 6.0 \times 10^{-3}$ at 232 s.

have also extracted the degree 2 part of these maps. We note that the zones of attenuation maxima that we observe in the central/eastern Pacific and over Africa/Red Sea correspond to the zones of attenuation maxima in *Durek et al.*'s [1993] maps at comparable periods (240 s, 160 s; e.g., Figures 9 and 11 of *Durek et al.*).On the other hand, *Suda et al.* [1991] have measured degree 2 attenuation for fundamental spheroidal modes of low frequency, sensitive to transition zone structure. The location and size of their degree 2 heterogeneity in Q is in good agreement with the degree 2 map extracted at 232 s. It is also in good agreement with even degree maps, which we have previously published [*Romanowicz*, 1990] using a different measurement method.

In the second step, an inversion with depth is performed at each point on the grid, relating the suite of attenuation coefficients at the set of periods given above to the Q_β structure at depth, using the relation [e.g., *Anderson et al.*, 1965;*Lee and Solomon*, 1979]:

$$Q_R^{-1}(T) = \int_0^a \left(\frac{\alpha}{T}\frac{\delta T}{\delta \alpha} Q_\alpha^{-1} + \frac{\beta}{T}\frac{\delta T}{\delta \beta} Q_\beta^{-1}\right) r^2 dr \qquad (1)$$

where α and β are compressional and shear velocities, respectively, and we assume that Q_κ is very large in the upper mantle, so that Q_α^{-1} is related to Q_β^{-1} by [e .g., *Deschamps*, 1977]:

$$Q_\alpha^{-1} = \frac{4\beta}{3\alpha} Q_\beta^{-1} \qquad (2)$$

In this process, we again use the approach of *Tarantola and Valette* [1982], and, instead of specifying a parametrisation with depth in terms of layers or polynomial coefficients, we introduce a correlation length relating two radii in the depth range 80 to 650 km. This correlation length increases with depth (from 50 km at the top to 200 km at the bottom of the upper mantle), reflecting the widening shape of the partial derivatives of Q_R. The input errors at each period are those obtained as output errors in the first step of the inversion. In this inversion step 49% variance reduction is obtained, for an inversion in which we solve for lateral heterogeneity in the depth range 80-650 km. Figure 4 shows the results, in terms of variance reduction, when the depth range is progressively increased from 80-250 km to 80-750 km. Below the maximum depth, the model is not perturbed from the Preliminary Reference Earth Model [PREM, *Dziewonski and Anderson*, 1981]. The variance reduction increases significantly as the maximum depth increases from 250 to 550 km, and beyond that, the improvement becomes marginal. We will be presenting our model down to 650 km (the bottom of the upper mantle), with the understanding that our data have weak sensitivity at depths below about 550 km. In this inversion process, we assume that we are in the middle of the absorption band, so that Q_μ is independent of frequency, and the frequency dependence of Q_R is entirely due to depth dependence of Q_μ.

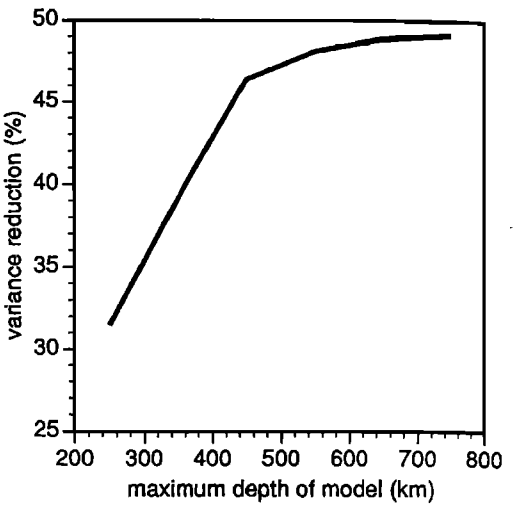

Figure 4. Variance reduction as a function of the maximum depth to which lateral heterogeneity is allowed to persist in the model.

Model Description

In Figure 5, we present the spherically symmetric part of our Q model (hereafter referred to as QR19), and compare it to other available radial Q models. In the depth range of our inversion (80-650 km), QR19 is in good agreement both with PREM [*Dziewonski and Anderson*, 1981] and a more recent model, QL6 [*Durek and Ekstrom*, 1994]. Like QL6, it has slightly lower Q than PREM in the low-Q zone (80-220 km) and slightly higher Q than PREM in the transition zone. It is smoother than either of these models because of the "continuous" parametrisation with depth. The discrepancies with model QM1 [*Widmer et al.*, 1991] reflect the discrepancies in the measurements of fundamental spheroidal mode Q, where larger Q values are obtained using complex amplitude fitting of free oscillations as compared to amplitudes of surface wavetrains [paper 1; J.J. Durek and G. Ekstrom, unpublished manuscript, 1994].

Samples of the complete 3D model are presented in Plate 1 at representative depths, and errors are illustrated in Figure 6. The coefficients of a degree 6 spherical harmonics expansion of this model are given in Table 1. Our model is originally presented by specifying values of Q^{-1} over a 10° by 10° grid of the Earth (that grid is arbitrary), but in Table 1, we have expanded it in spherical harmonics up to degree 6 for easier comparison with other tomographic results as presented in the literature. Since this is the first complete three-dimensional Q model of the upper mantle, comparison with other models is not possible and the complete validation of this model will have to await confirmation by independent studies: other studies of global Q distribution in the upper mantle [*Durek et al.*, 1993; *Suda et al.*, 1991] have only addressed the question of even degree features of lateral variations in Q and have only presented maps at constant period.

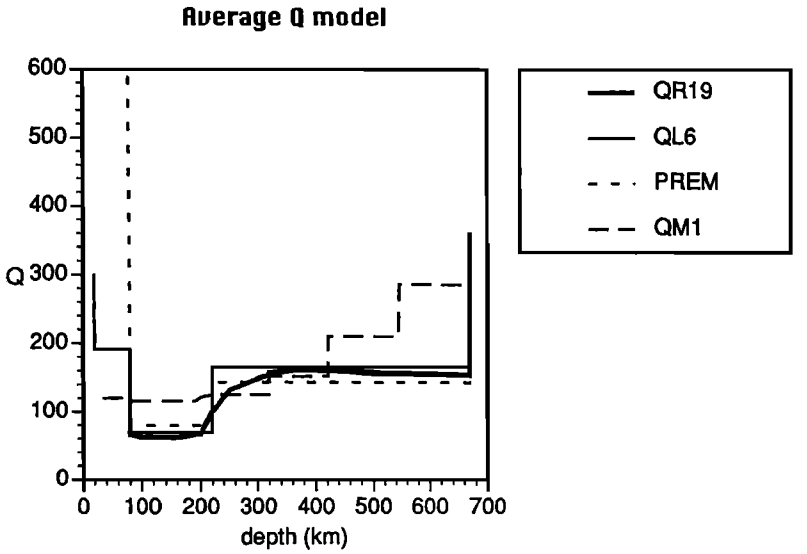

Figure 5. Spherically averaged Q model (thick line) as compared to other available models: PREM [*Dziewonski and Anderson*, 1981], QM1 [*Widmer et al.*, 1991] and QL6 [*Durek and Ekstrom*, 1994].

In Plate 1, we note a change of pattern in Q heterogeneity between the uppermost mantle (down to 250 km) and mid-upper mantle to transition zone depths. In the uppermost mantle, the pattern is well correlated with tectonic features, particularly so around 200 km. High attenuation is found in oceanic regions: we recognize high-attenuation regions over the central and southern part of the East Pacific Rise, over the central Indian ocean (the anomaly is slightly shifted to the north with respect to the ridge, which may be due to a resolution problem), and over the northern and southern mid-Atlantic Ocean, in agreement with results of recent regional studies [*Sheehan and Solomon*, 1992; *Ding and Grand*, 1993]. The only non oceanic high-attenuation zone, located over the western Pacific subduction zones, can be associated with back arcs, since very high attenuation has been documented in these regions [*Nakanishi*, 1979;*Revenaugh and Jordan*, 1989; *Flanagan and Wiens*, 1990]. A zone of high attenuation in the central Pacific, which becomes stronger with depth, is perhaps the only unexpected feature on the basis of comparison with surface tectonics as well as upper mantle elastic tomographic models. Low attenuation over western Africa and western Eurasia, seen particularly clearly in the maps at 200 and 250 km, corresponds to regions of high S velocity in recent elastic tomographic models [*Montagner and Tanimoto*, 1992; *Su et al.*, 1994]. Antarctica, Australia, and parts of North and South America are also characterized by relatively low attenuation (high Q). At depths beyond 300 km, the pattern changes, with a shift to the west of the zones of high attenuation, in the central Pacific on the one hand, and in Indian Ocean/Africa on the other, where the anomaly previously located in the middle of the Indian Ocean has moved over northern Africa and the Red Sea region. The general shift of the pattern of heterogeneity towards the west is in good correspondence with a well documented shift in pattern of elastic structure apparent in all upper mantle global elastic models [*Montagner and Tanimoto*, 1992; *Su et al.*, 1994]. It is particularly clear in the degree 2 pattern of the model, shown in Figure 7 at depths of 250 km and 370 km. Because of the significant variance reduction obtained by considering 3D Q structure below 300 km as indicated in Figure 4 and because of the results of resolution tests presented in the next section, we believe this change of pattern around 250-300 km depth in the Q maps is significant.

At depths greater than 300 km, we have superimposed the distribution of hotspots according to *Richards et al.* [1988] on the Q maps. We note that all except a few hotspots are located in zones of higher than average attenuation at mid-upper mantle depths. This correspondence with hotspots in the transition zone was already noted for degree 2 in the work of *Suda et al.* [1991]. We have discussed the issue of correlation with hotspot distribution extensively in a separate publication [*Romanowicz*, 1994b], and in particular have argued that it is important to appropriately weigh the hotspot distribution, namely according to buoyancy strength in order to perform a comparison with the Q tomography. In particular, this weighting has the consequence of emphasizing the Pacific and African hotspots relative to others, such as, for example, north Atlantic hotspots. The pattern of heterogeneity in Q appears to shift from one correlated with tectonic features in the shallow upper mantle to one correlated with hotspot distribution at greater depths. In Figure 8, we plot the correlation of model QR19 with , on the one hand, heat flow, and, on the other, the hotspot distribution [*Richards et al.*, 1988], with the latter weighted according to buoyancy strength [*Sleep*, 1990]. Significant correlation switches from heat flow (itself well correlated with ridges) to hotspots in the depth range 200-300 km,

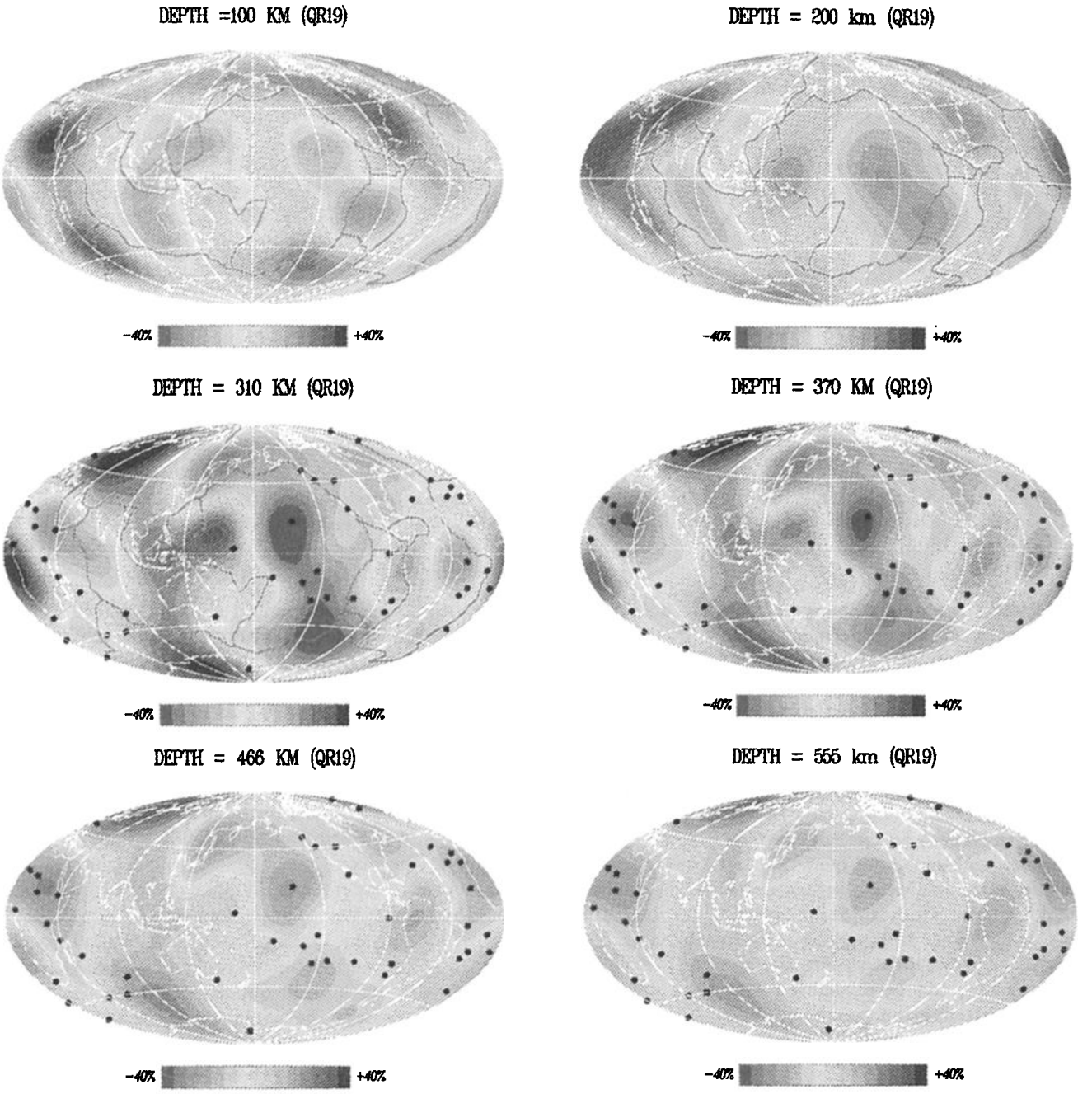

Plate 1. Horizontal cross sections showing model QR19 at different depths in the upper mantle. The lateral variations are expressed in terms of relative variations in Q with respect to the average in the layer: orange and blue indicates regions of high and low attenuation, respectively. At depths greater than 300 km, the distribution of hotspots according to *Richards et al.* [1988] is shown, indicating correlation with regions of low Q.

whereas a similar plot for elastic structure indicates increased correlation with slab distribution below 300 km [e.g., *Romanowicz*, 1994b] . The variance reduction plot shown in Figure 4 indicates that this is well within the range where heterogeneity is required by the data. At depths greater than 450 km, the level of heterogeneity seems to decrease, while retaining a similar pattern. It is difficult to determine how significant this is, given the limited sensitivity of fundamental mode Rayleigh waves to structure deeper than 550 km, although error maps (Figure 6) indicate that the peaks in attenuation in the central Pacific and northern Africa are significant down to 650 km.

In what follows we address more thoroughly issues of resolution, and in particular the question of contamination by unmodelled effects of elastic structure in the amplitudes.

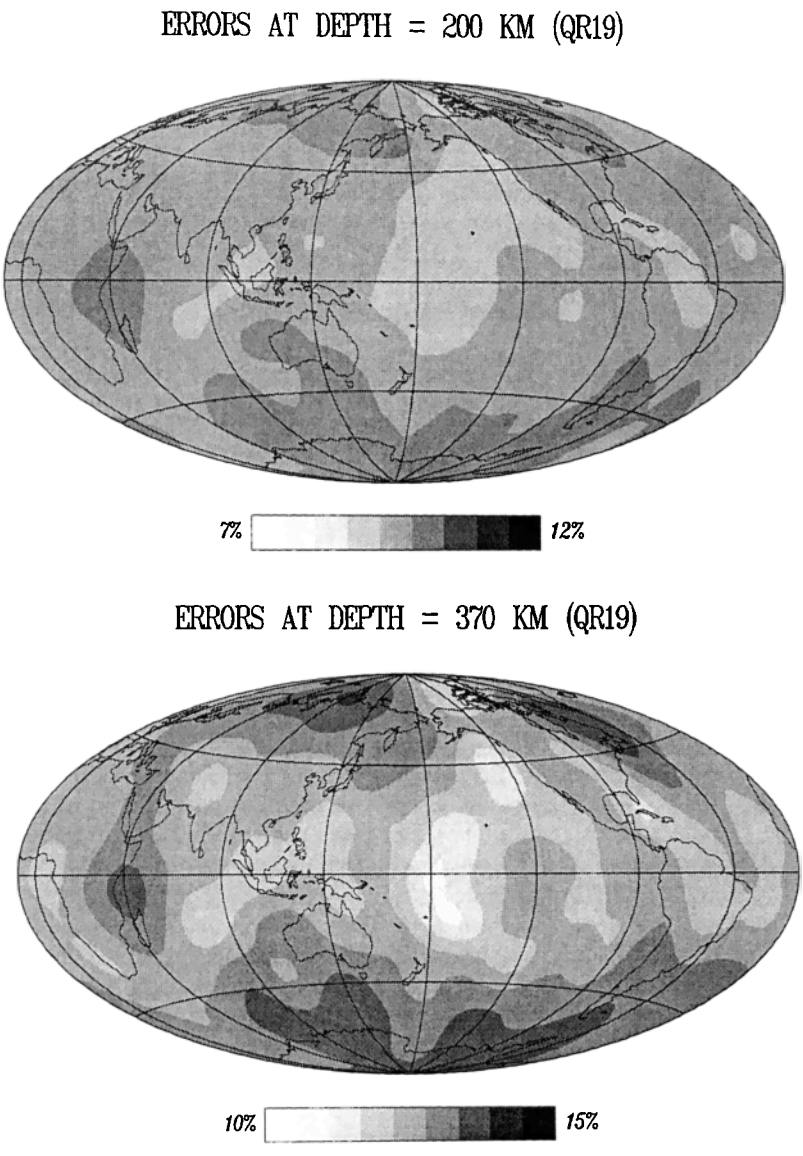

Figure 6. Examples of error maps at two characteristic depths: 200 km and 370 km. Error maps at other depths have similar structure, with errors ranging from 20-25% at 100 km, 15-18% at 310 km, 8-12% at 466 km, to 9-12% at 555 km.

Addressing Resolution Issues

Spatial and Depth Resolution

We have assembled a synthetic data set of attenuation coefficients, measured for the same path distribution as in the actual data set, for a model of shear attenuation in the upper mantle consisting of a checkerboard pattern confined to a layer located successively in three depth ranges: 150-250 km, 250-450 km, and 450-650 km. In the examples shown here, the checkerboard pattern was generated using a spherical harmonic of degree l=6 and order m=4. These synthetic data sets were inverted, following the same approach as that used with the actual data (in particular the same damping parameters), in order to assess how well the checkerboard pattern could be recovered, both spatially and in depth. Figure 9 shows the results of the inversions. The spatial checkerboard pattern is satisfactorily resolved in all three cases. As for the depth resolution, all three input layers are also well recovered, with little leakage into neighboring layers. This is not unexpected, given the continuous parametrization used in the inversion with depth, which cannot perfectly accommodate the sharp character of the input layer boundaries.

The results of these tests show that, with the data coverage and the frequency range considered, it is possible to resolve lateral heterogeneity of wavelength equivalent to a degree 6 spherical harmonic and distinguish its location with depth within three depth ranges in the upper mantle. In particular, differences in patterns of lateral heterogeneity observed in the first 250 km of the

Table 1. Coefficients of a Degree 6 Spherical Harmonics Expansion of the Tomographic Q Model Presented in Plate 1

	depth, km																	
	647		511		422		370		310		250		200		160		100	
lm	C	S	C	S	C	S	C	S	C	S	C	S	C	S	C	S	C	S
00	67.1		66.2		65.1		65.2		67.8		76.6		145.3		154.9		153.5	
10	0.72		0.82		1.00		1.01		0.77		0.06		-0.82		-1.20		-0.56	
11	0.11	-0.67	-0.14	-1.30	-0.72	-2.52	-1.44	-3.66	-2.91	-5.34	-5.16	-6.82	-6.71	-6.25	-6.23	-3.73	-2.64	0.63
20	-1.06		-1.03		-1.01		-0.81		-0.32		0.26		0.04		-1.17		-3.58	
21	-0.18	0.26	-0.28	0.29	-0.50	0.38	-0.70	0.47	-0.99	0.65	-1.27	1.05	-1.23	1.61	-0.86	2.00	-0.17	1.97
22	1.97	0.98	1.95	1.50	1.93	2.44	1.46	3.16	0.09	3.81	-2.29	3.37	-3.88	0.84	-3.10	-2.38	1.35	-5.26
30	-1.61		-1.63		-1.60		-1.12		0.39		3.37		6.15		6.50		2.67	
31	-1.42	-1.65	-1.91	-2.02	-2.75	-2.75	-3.19	-3.16	-3.11	-3.31	-1.23	-2.54	2.68	-0.66	6.19	1.15	7.39	2.05
32	0.67	-0.33	0.69	-0.54	0.79	-0.94	0.80	-1.30	0.81	-1.78	-2.12	2.09	-1.71	3.33	-0.67	4.55	0.97	
33	0.17	0.26	-0.20	0.09	-0.78	-0.38	-1.29	-1.13	-1.74	-2.84	-0.96	-5.87	2.20	-8.42	6.15	-8.40	9.74	-4.05
40	-0.63		-0.80		-1.10		-1.27		-1.29		-0.83		0.13		0.98		1.24	
41	-1.44	-0.02	-1.67	0.14	-2.06	0.41	-2.06	0.67	-1.34	1.01	0.96	1.10	4.26	0.44	6.34	-0.69	5.52	-2.08
42	-0.02	-1.08	-0.03	-1.23	0.01	-1.56	0.11	-1.72	0.49	-1.78	1.50	-1.77	3.01	-1.97	4.15	-2.52	4.29	-3.61
43	0.38	-0.21	0.36	-0.12	0.35	-0.02	0.26	0.06	0.02	0.09	-0.37	-0.27	-0.58	-1.20	-0.41	-2.15	0.32	-2.68
44	-0.53	-0.13	-0.81	-0.16	-1.30	-0.22	-1.64	-0.26	-1.84	-0.33	-1.24	-0.49	0.53	-0.79	2.42	-1.11	3.62	-1.38
50	0.12		0.32		0.66		0.97		1.32		1.31		0.42		-0.87		-2.21	
51	-0.18	0.00	-0.34	-0.17	-0.58	-0.48	-0.74	-0.80	-0.75	-1.26	-0.13	-1.59	1.35	-1.23	2.85	-0.29	3.71	1.13
52	-1.00	-0.59	-1.05	-0.97	-1.15	-1.66	-0.99	-2.23	-0.37	-2.85	0.97	-2.84	2.34	-1.39	2.70	0.74	1.26	2.94
53	-0.18	0.40	-0.09	0.67	0.17	1.14	0.55	1.49	1.43	1.78	2.95	1.45	4.20	0.07	4.15	-1.52	1.94	-2.65
54	0.25	-0.06	0.37	0.18	0.54	0.61	0.57	1.03	0.32	1.60	-0.80	1.82	-2.75	0.86	-4.37	-0.84	-4.75	-2.95
59	-0.30	-0.58	-0.37	-0.69	-0.52	-0.89	-0.61	-0.95	-0.67	-0.81	-0.61	-0.25	-0.35	0.51	-0.04	0.87	0.24	0.31
60	-0.03		-0.14		-0.35		-0.54		-0.75		-0.66		0.17		1.38		2.75	
61	-0.22	-0.17	-0.17	-0.08	-0.06	0.09	0.10	0.30	0.43	0.66	0.83	1.04	0.86	0.96	0.36	0.36	-0.84	-0.83
62	0.06	-0.55	-0.03	-0.65	-0.18	-0.86	-0.31	-0.94	-0.46	-0.89	-0.38	-0.47	0.21	0.24	1.02	0.75	1.82	0.73
63	-0.33	-0.02	-0.31	-0.19	-0.25	-0.51	-0.08	-0.81	0.35	-1.25	1.12	-1.48	1.75	-0.85	1.70	0.43	0.52	2.24
64	-0.49	0.12	-0.50	0.18	-0.51	0.28	-0.39	0.33	0.03	0.32	0.94	0.07	1.94	-0.47	2.33	-0.95	1.60	-1.13
65	0.54	-0.34	0.50	-0.47	0.44	-0.72	0.27	-0.90	-0.13	-1.08	-0.67	-1.08	-0.74	-0.76	-0.09	-0.34	1.51	0.01
66	-0.27	0.03	-0.43	0.10	-0.69	0.23	-0.88	0.38	-0.99	0.64	-0.72	0.93	0.10	0.96	0.92	0.65	1.29	-0.08

Coefficients are given in terms of Q^{-1}. The expansion is as follows $Q^{-1} = [C_{00} + \sum_l \sum_m (C_{lm} cos m\phi + S_{lm} sin m\phi) plm$, where *plm* are fully normalized associated Legendre functions [e.g., *Woodhouse and Dziewonski*, 1984]

upper mantle and those observed at greater depth must reflect realistic variations of structure with depth.

Given that the partial derivatives of Q_R with respect to structure are closely related, in their depth dependence, to those of Rayleigh wave phase velocity, these results are not surprising, since it has been widely documented in the literature that low frequency fundamental model Rayleigh wave data can resolve the equivalent of about three layers of heterogeneity in the upper mantle [e.g.,*Anderson et al.*, 1965; *Tanimoto*, 1986; *Montagner and Tanimoto* 1991].

Perturbations Due to Elastic Structure

Much more specific to the problem of Q tomography, and the subject of much debate, is the issue of contamination of attenuation data by effects of propagation in an elastic 3D Earth. As mentioned in paper 1, we believe that the present 3D elastic models of the mantle are not constrained well enough in their short wavelength features to allow accurate forward modelling of focussing/defocussing effects in the amplitudes that could be used as corrections before inversion for Q structure. Indeed, such effects depend on first and second transverse derivatives of elastic structure along the travel path, which are, in turn, particularly sensitive to sharp features in the elastic structure. In terms of spherical harmonics expansions, for each c_{lm} coefficient of degree l and order m of the elastic structure, the second derivatives will be proportional to $l^2\ c_{lm}$, emphasizing higher degree terms. Because their higher degree terms are not accurate, current 3D elastic models fail, in many instances, to reproduce actually observed patterns of amplitude anomalies, especially when these are large. Figure 10 shows the results of an attempt to synthetically produce large band-limited fluctuations in the amplitude, such as those shown in Figure 2b, by

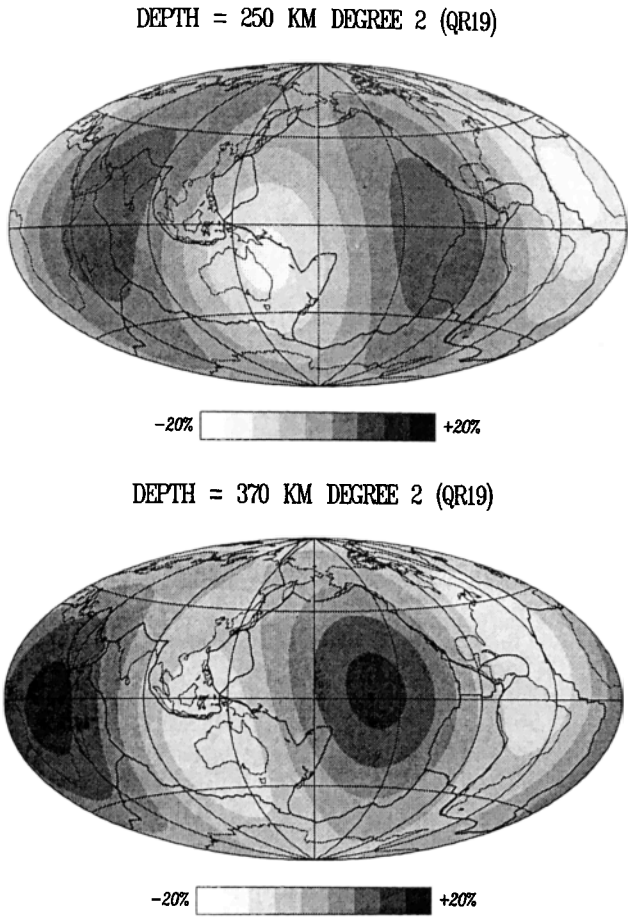

Figure 7. Degree 2 maps of $\delta Q^{-1}/Q^{-1}$ extracted from model QR19 at 250 km and 370 km depths.

calculating focussing effects on the corresponding path, for a recent upper mantle 3D elastic model [*Montagner and Tanimoto*, 1992]. The band-limited character and strength of amplitude fluctuations with period can only be reproduced, even qualitatively, by increasing transverse derivative terms that enter the expression of focussing perturbations, by a factor of 2 or 4. This was also illustrated previously in Figure 4 of *Romanowicz* [1987].

In the absence of a more sophisticated and valid quantitative method to deal with focussing effects, our philosophy is therefore to apply drastic data selection criteria, eliminating those paths which appear strongly contaminated by focussing effects, as already described above. The main deficiencies of this approach are that (1) 70-80% of the analyzed data are rejected, which eventually limits spatial resolution; (2) only smooth variations of amplitude with frequency are kept, so that, if large localized heterogeneity in Q is present, it cannot be resolved; and (3) some focussing effects that appear smooth as a function of frequency may insiduously contaminate the data.

Deficiencies 1 and 2 explain why we are not able to propose an upper mantle Q model equivalent in resolution to currently available elastic models. On the other hand, deficiency 3 can be tested to determine how much contamination by unmodelled smooth elastic effects is to be expected.

Two types of tests were conducted. In the first series of experiments, synthetic seismograms were calculated by the variational method (S. Watada, personal communication, 1994) for the same paths as those used in the "real" inversion. The model consisted of the spherically symmetric Q distribution of the PREM model [*Dziewonski and Anderson*, 1981] and the elastic model SH12/WM13 [*Su et al.*, 1994]. These seismograms were

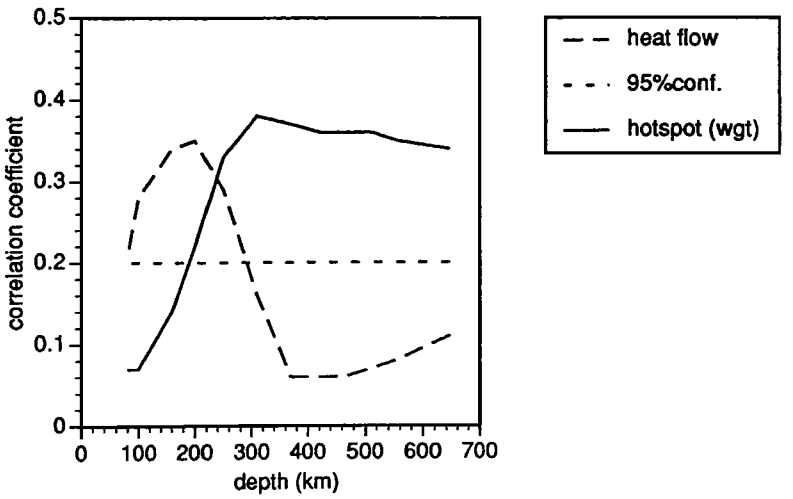

Figure 8. Correlation of model QR19 with heat flow [*Chapman*, 1985] and hotspot distribution [Richards et al., 1988], as a function of depth. The 95% confidence limit for the calculation of the correlation coefficient, using spherical harmonics expansions up to degree and order 6, is shown. The hotspot distribution is weighted according to buoyancy strength as evaluated by *Sleep* [1990]. See *Romanowicz* [1994b] for a more detailed discussion.

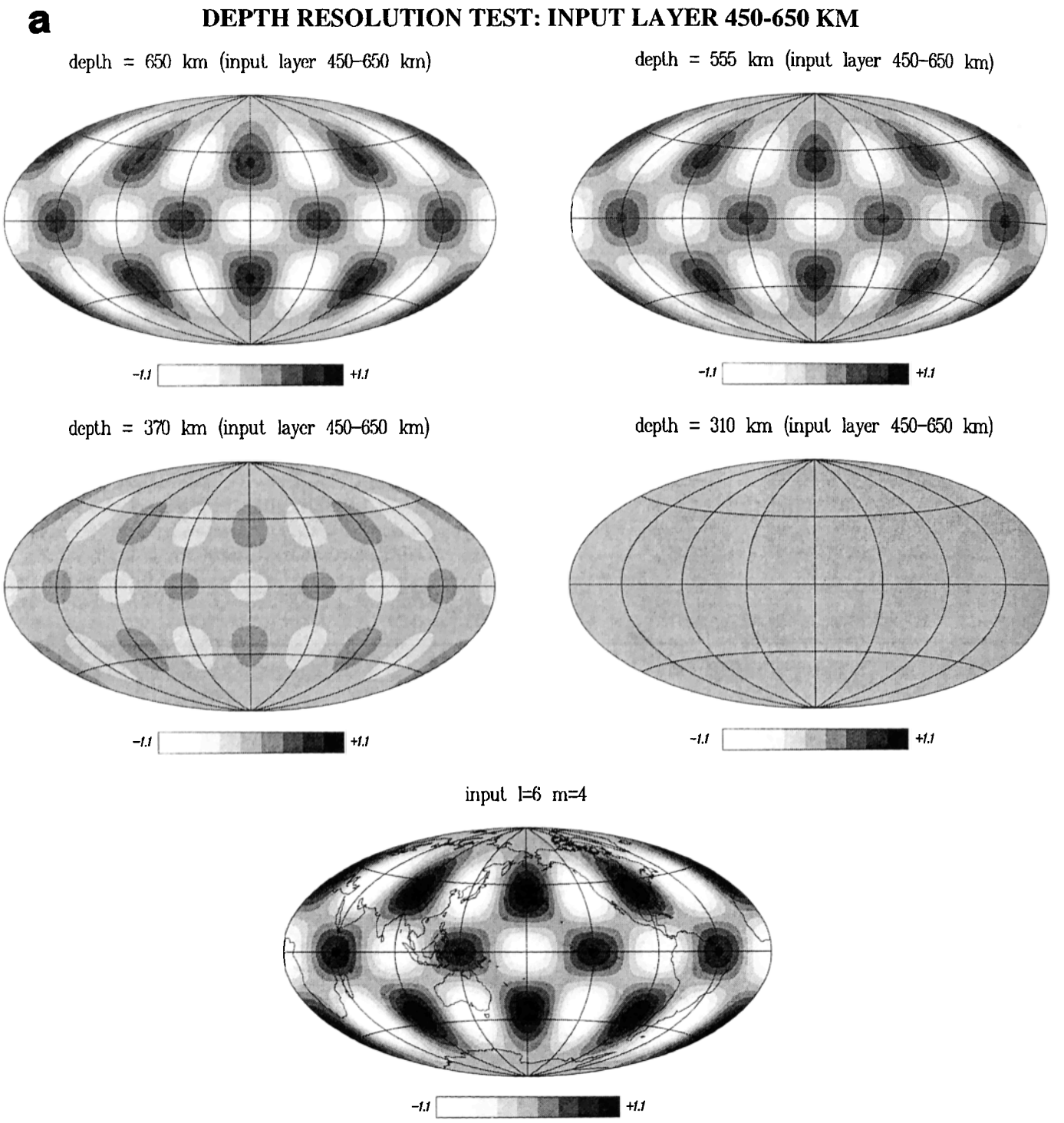

Figure 9. Results of a checkerboard test for depth resolution. The input model is a layer with heterogeneity in Q described by a spherical harmonic function of degree 6 and order 4, as shown in a), located respectively between depths of (a) 450-650 km , (b) 250-450 km and (c) 150-250 km. Synthetic Q_R anomalies are computed for the frequency band corresponding to our real data set, and then reinverted, using the same procedure as with real data, for a model of heterogeneity confined between depths of 80 and 650 km. The inverted model is shown, in each case, at different depths within and outside of the depth range of the input layer, showing that in all three cases leakage outside of the input layer is not significant.

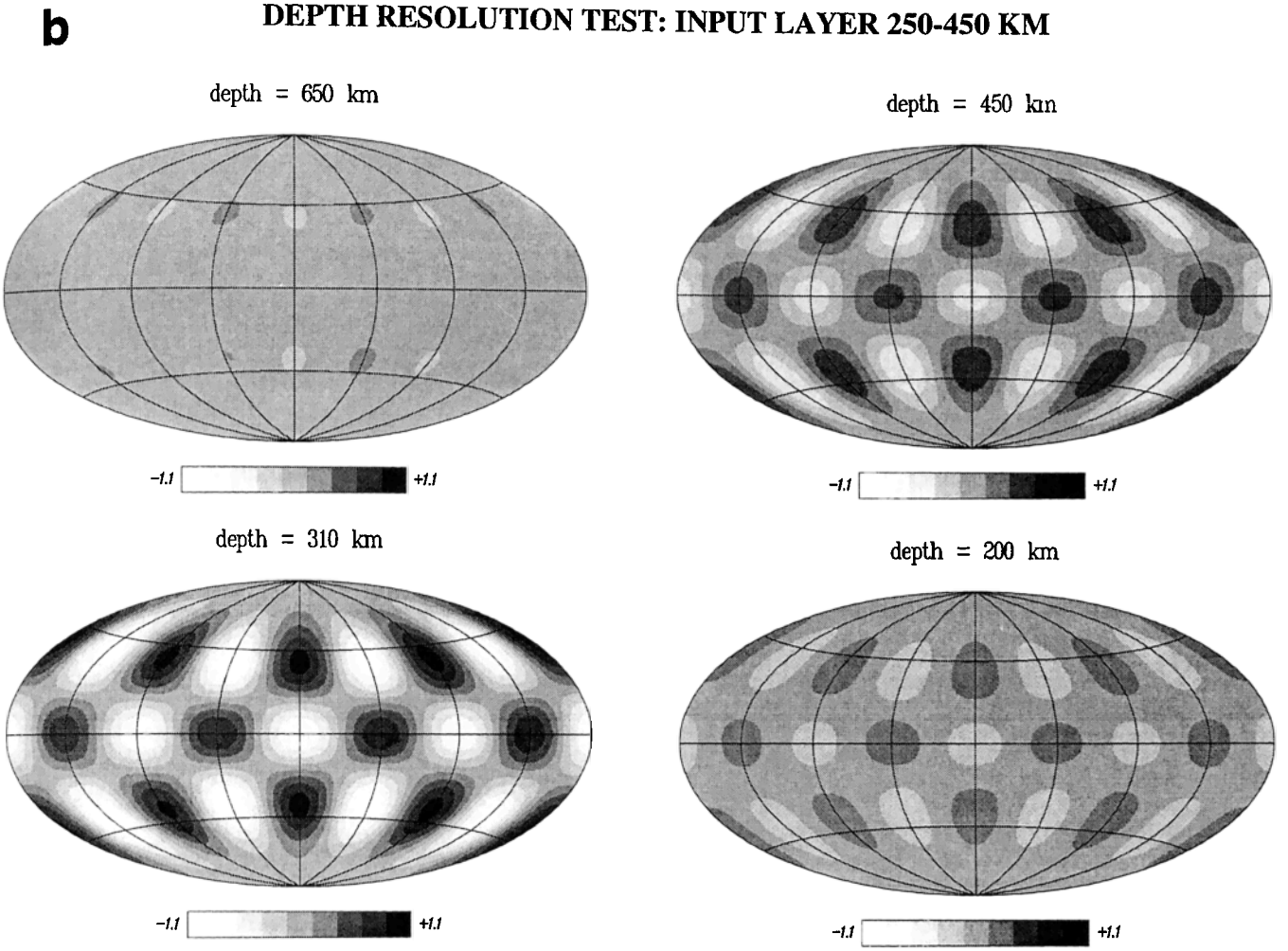

Figure 9. (continued)

then analyzed using the same procedure as with the real data, assuming in particular that the smooth departures from PREM in the amplitudes were due to anelastic structure. Simulated "anelastic" maps were thus obtained at different periods and compared to the actual maps. Examples are shown in Figure 11, at periods of 200 s and 160 s. One can see that the maps based on real data do not have much in common with the maps obtained with the synthetic data set, demonstrating that the observed heterogeneity is not likely to be the result of mapping focussing effects into artificial lateral variations in Q, inasmuch as we are able to synthetically produce realistic mild focussing effects. We note however, that the "false" Q maps show lateral variations which are not insignificant. This has led us to the next experiment, in which we have constructed a synthetic data set of attenuation coefficients by adding synthetically computed focussing effects to our actual two-dimensional (2D) Q maps, at periods of 160 s and 200 s respectively. We subsequently reinverted these data sets, assuming that the total amplitude anomaly was due solely to Q. The resulting inverted maps are shown in Figure 12 where they compared to the original 2D Q maps. We see that most of the original 2D Q features are well recovered and the most perceptible difference is in the back of the western Pacific subduction zones, where strong lateral variations in elastic velocity due to the slabs are the likely source of strong gradients of structure.

Finally, a last set of tests consisted in adding focussing effects calculated, this time, using the upper mantle model of *Montagner and Tanimoto* [1992] and higher order asymptotic theory [*Romanowicz*, 1987], to a checkerboard pattern of heterogeneity in Q. This is a very extreme test, given that the character of lateral heterogeneity in Q is very different from that of the focussing effects: by the nature of the checkerboard pattern, the averaging which occurs when adding effects of the Q model over long source station paths results in amplitude anomalies that can be small compared to the focussing anomalies, calculated for a model that does not have this type of regularity. Therefore, the "observed" amplitude anomalies are, on some paths, dominated by the more realisitically distributed focussing effects. In Figure 13, we present the results of several inversions in which we successively reject paths that

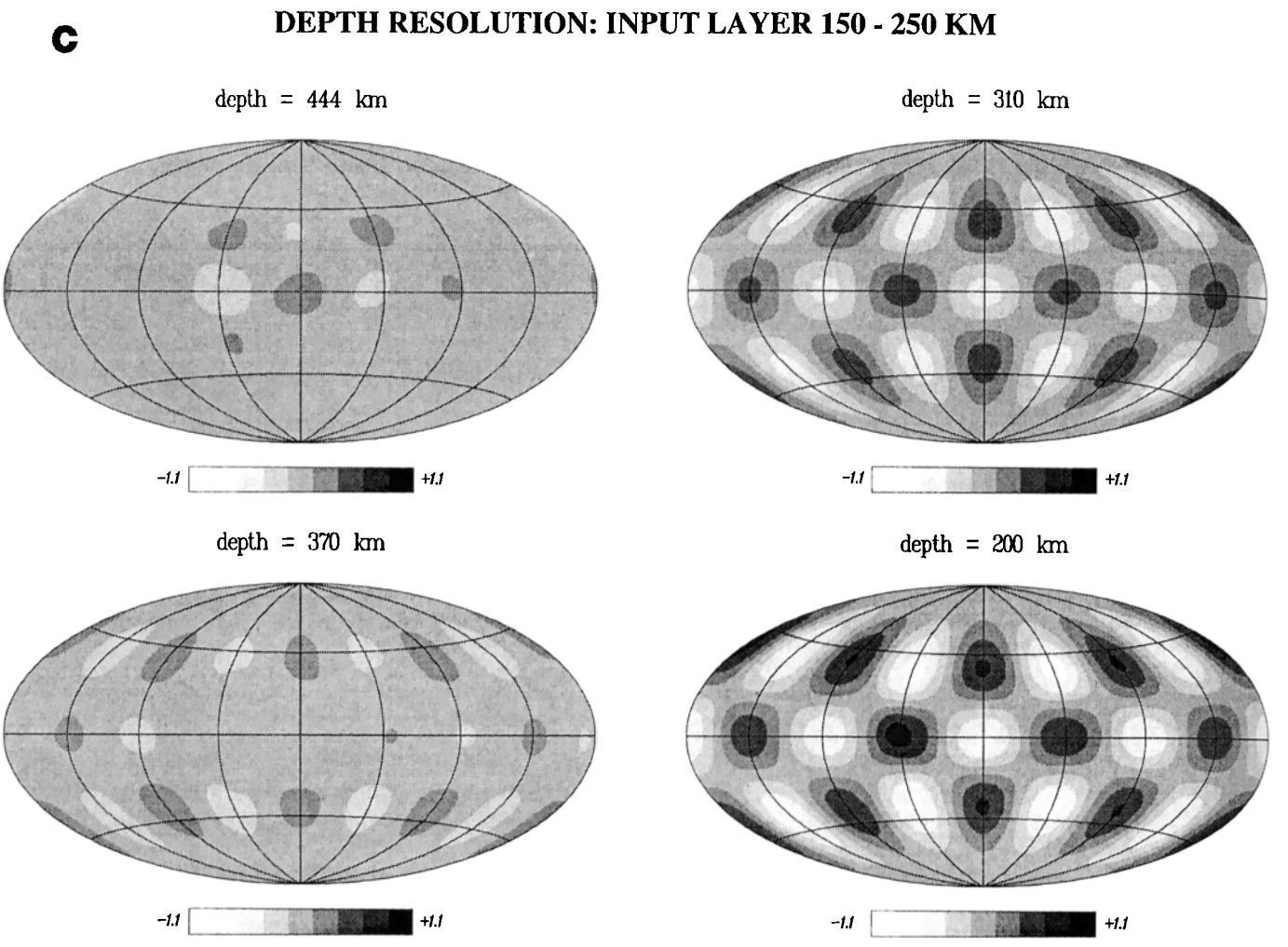

Figure 9. (continued)

contain focussing anomalies that are larger by a given factor f than the corresponding attenuation anomalies. We see that for values of f up to 2, the checkerboard pattern is well recovered. If all paths are kept, the recovered pattern exhibits some smearing of the checkerboard, and also the maximum amplitudes, in some regions, are larger by a factor of 1.5 compared to the input amplitudes. The difference between Figure 13e and Figure 13f represents about 10% additional paths in the latter, including some for which the ratio f is larger than 10. This is a worst case situation, since in practice, paths for which such large amplitude anomalies might be present would be eliminated in the course of the severe data selection procedure.

In conclusion, our tests indicate that, while some residual focussing effects may be present in our attenuation data set in spite of the rigorous selection criteria, they will not dominate the final pattern of 3D heterogeneity in Q. We believe that this encouraging result can be related to the difference in the way in which attenuation anomalies and focussing anomalies are accumulated along the propagation path. Attenuation anomalies are additive, regardless of the direction of travel, and the attenuation structure is a scalar property attached to each location. Focussing anomalies, on the other hand, depend on the direction of approach (transverse derivatives along the propagation path). In a tomographic inversion scheme designed to extract local scalar properties of the medium, the latter will tend to be eliminated in favor of the former.

Discussion and Conclusions

We have presented a 3D Q model in the upper mantle which is the first of its kind. This model is clearly very preliminary and the details of the patterns will likely change as our abitility to gain resolution increases in the future. The numerous tests we have performed indicate, however, that the following large scale features are well resolved and do not represent an artifact due to contamination by elastic structure: (1) the persistance of lateral heterogeneity in Q into the transition zone and (2) the change in spatial pattern, around 300 km, from one correlated with surface tectonics and heat flow at shallow depth, to one correlated with the distribution of hotspots at transition zone depths.

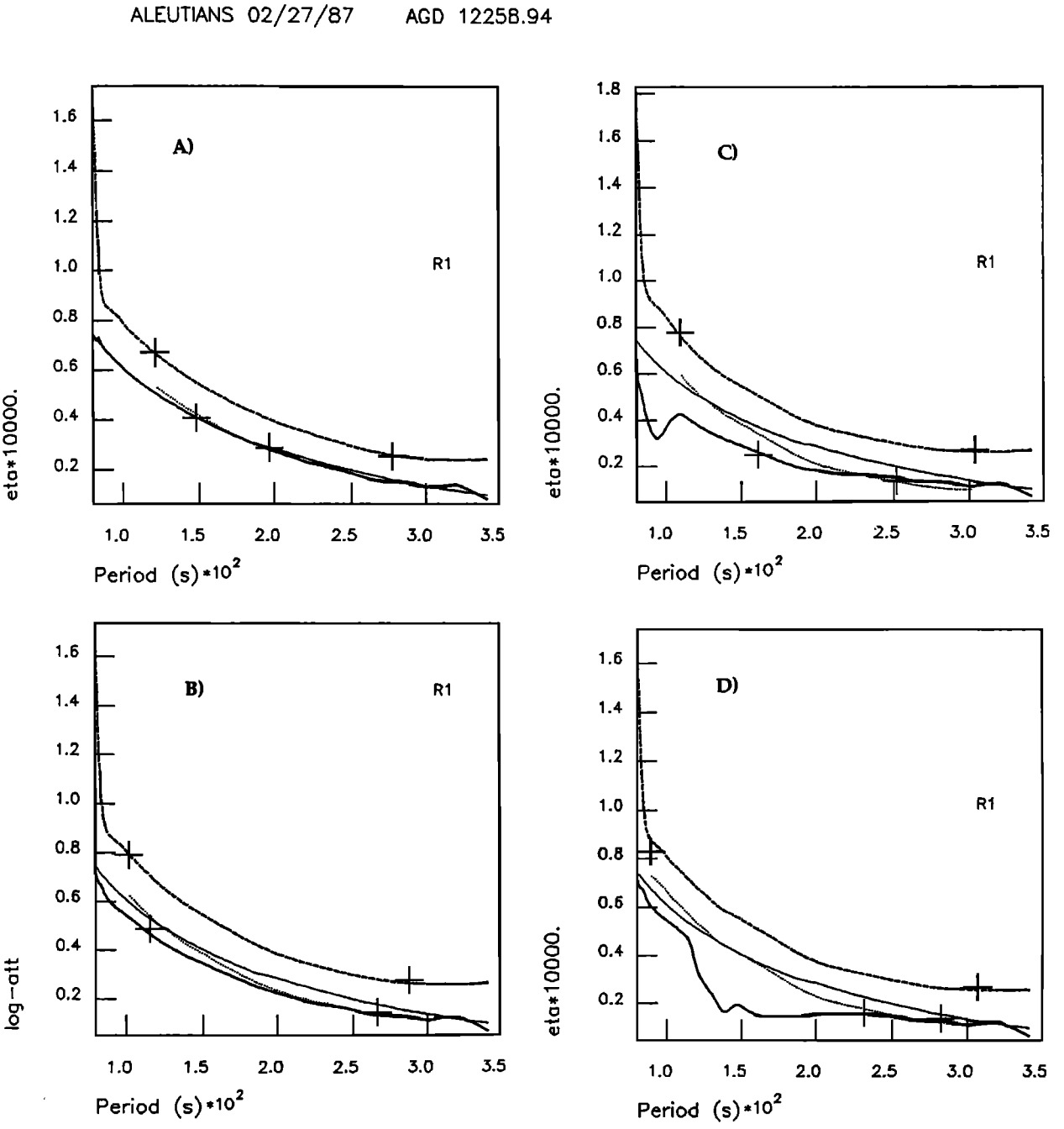

Figure 10. Plots of attenuation coefficient as a function of period, as in Figure 2, but for a synthetic experiment corresponding to the path of Figure 2b. Retrieved attenuation coefficient plots are: (a) for the input Q PREM model, which is correctly retrieved and (b) when we add focussing terms to the Q model, calculated using higher order asymptotic theory, for the upper mantle model of *Montagner and Tanimoto* [1992]. The retrieved attenuation coefficient is shifted smoothly, as a function of frequency, with respect to PREM. (c) same as (b), but we have modified the input elastic model by multiplying the transverse gradients on the path considered by a factor of 2 in the period range 120-250 sec and by a factor of 4 in the period range 90-120 sec; (d) same as (b) and (c) but the transverse gradients have been multiplied by a factor of 2 in the period ranges 120-140 sec and 190-220 sec and by a factor of 4 in the period range 140-170 sec. A band-limited effect qualitatively similar to what is observed appears in the determination using R1R2R3, resulting in a final measurement (dotted line), shifted with respect to the input PREM model.

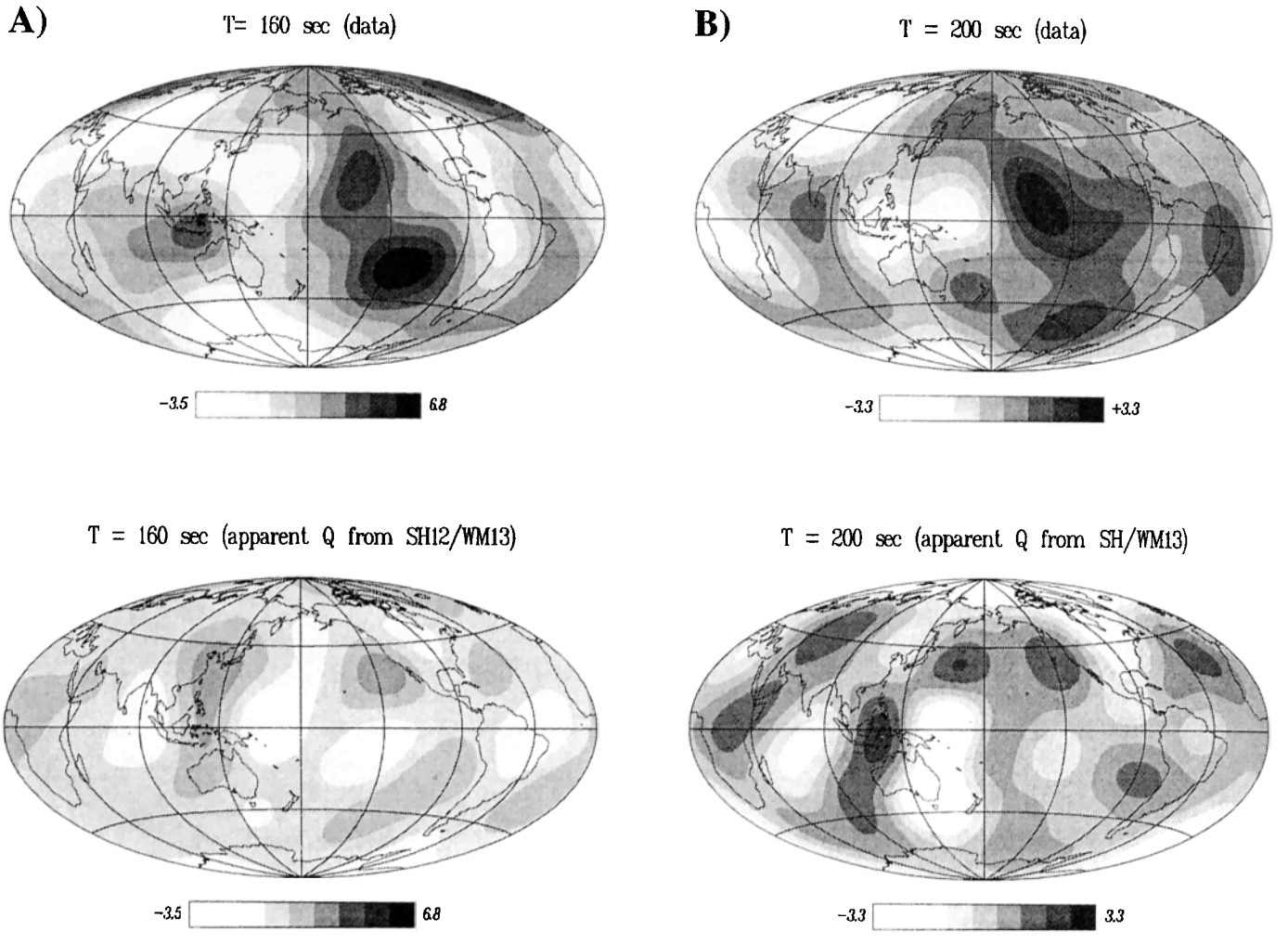

Figure 11. Comparison of observed maps of lateral variations in Q^{-1} (top figures) at periods of (a) 200 sec and (b) 160 sec with synthetic maps (bottom figures), obtained by assuming a spherically symmetric Q model (PREM) and an elastic 3D model [*Su et al.*, 1994] and inverting amplitude data for "apparent" lateral variations in Q.

Our data lack the resolution to be able to determine whether the fact that the deeper pattern, which seems to continue throughout the transition zone and which gradually decreases in relative amplitude with depth, is realistically retrieved below a depth of about 500 km. The consistency of the pattern needs to be confirmed by independent studies, using data with greater sensitivity to structure in this depth range.

The geodynamic implications of the main features of our model, assuming that lateral variations of Q primarily reflect thermal structure in the upper mantle. have been discussed in detail in a separate publication [*Romanowicz*, 1994b]. We briefly summarize them here. The pattern of lateral variations in Q at shallow depth, correlated with tectonic features and heat flow, is in good agreement with what would be expected from lithospheric plate cooling models. In particular, we have shown that Q, as obtained in model QR19, is correlated with age of oceanic plate, in the southern Pacific and southern Atlantic, down to about 250 km [*Romanowicz*, 1994b]. Below 300 km, a correlation with hotspots emerges, revealing two major "upwellings": one in the central Pacific related to the Hawaian hotspot and the group of hotspots associated with the south Pacific "superswell" [*McNutt and Fischer*, 1987; *Calmant and Cazenave*, 1986], and one under north Africa, associated with rifting and volcanism whose deep origin may be obscured by the passage through thick, cold, and chemically distinct continental lithosphere. These results point to the importance of further studying the characteristics of African hotspots from a geochemical point of view and indicate that Q tomography, if better resolution can be achieved, may eventually help to sort out the different origins and geodynamical importance

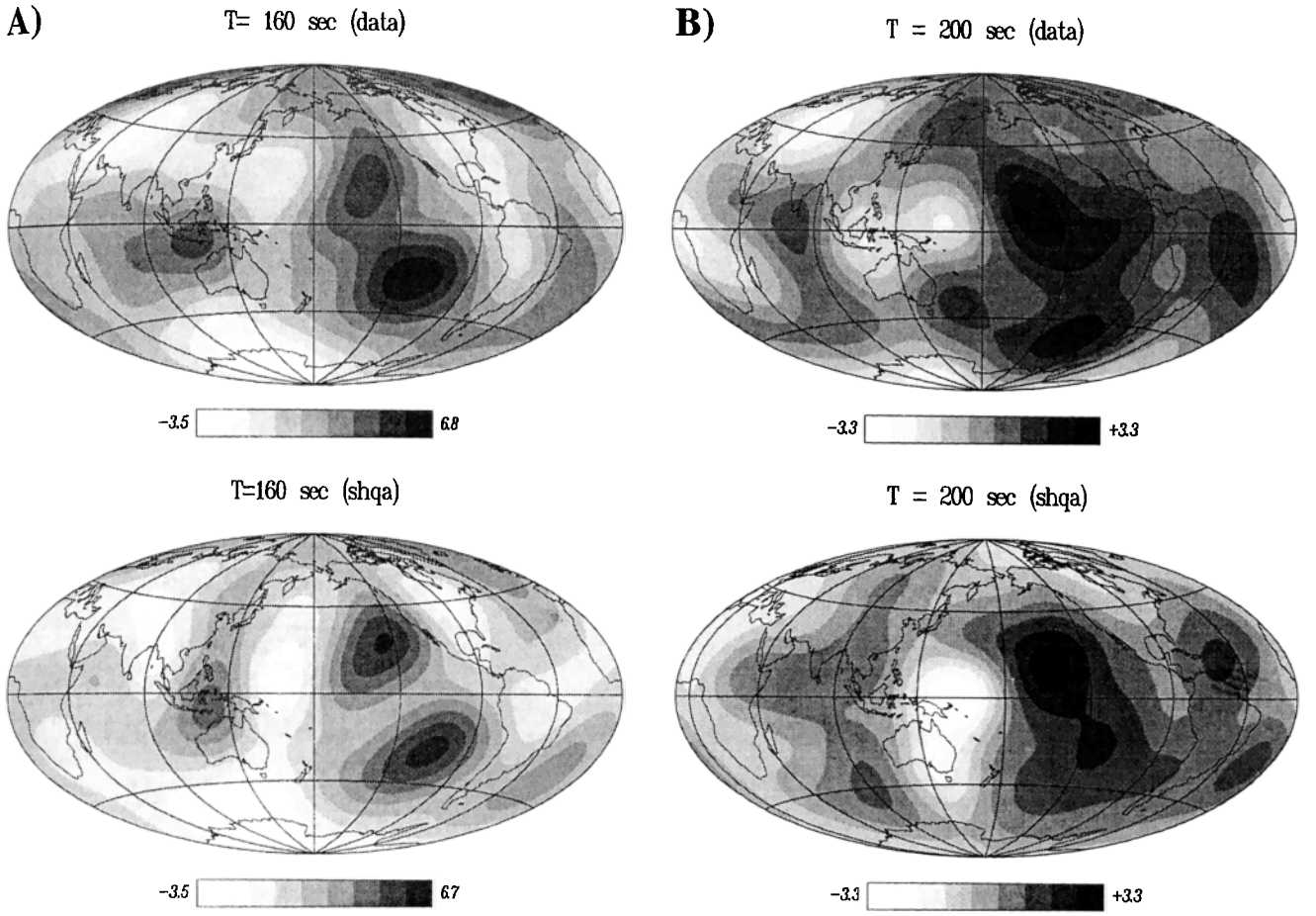

Figure 12. Comparison of actual maps (top figures) of lateral variations in Q^{-1} at periods of (a) 160 s and (b) 200 s, with the maps (bottom figures) obtained by inverting a synthetic data set of attenuation coefficients for the paths corresponding to our real data, in which we have added focussing effects computed using higher order asymptotics for the model of *Montagner and Tanimoto* [1992] to the amplitude anomalies produced by lateral variations in Q, as in (a). The inversion was performed assuming all of the effect in the amplitude was due to Q. The addition of focussing effects does not significantly alter the resulting Q map.

of groups of hotspots around the earth [*White*, 1985; *Kellogg and Wasserburg*, 1990].

The change of pattern at mid upper mantle depth is also seen in elastic models. However, we note that the Q tomography emphasizes different features of upper mantle structure than does velocity tomography: even the most recent degree 12 elastic models have a much weaker correlation, in the transition zone, with hotspots than with slabs [e.g., *Romanowicz*, 1994b]. This is as expected from considerations of comparative temperature dependence of Q and elastic velocities, as shown in Figure 1.

At this point, it is difficult to make definite inferences as to the morphology and depth of origin of hot upwelling currents, but our Q model appears to support the expected results of interaction of the deep global circulation with overlying plates [*Davies*, 1990; *Gurnis and Zhong*, 1991]: major upwellings ("plumes") rising from the deep mantle, not necessarily directly situated beneath ridges, broaden when encountering lithospheric plates and deflect the primary flow towards ridges, while narrow conduits through the lithosphere result in observed hotspots directly above the plume. Ridges would therefore be essentially passive features which "attract" the excess flow from plumes that cannot find their way to the surface, shielded by the lithosphere, which is cold and difficult to penetrate. According to model QR19, the widening of the plumes would be centered around a depth of 300 km ($\pm$100 km), where we observe the strongest Q heterogeneity and where there is also a documented peak in degree 2 elastic structure [e.g. *Romanowicz et al.*, 1987]. We believe it is worth to further improve resolution in Q tomography in order to confirm and refine these results.

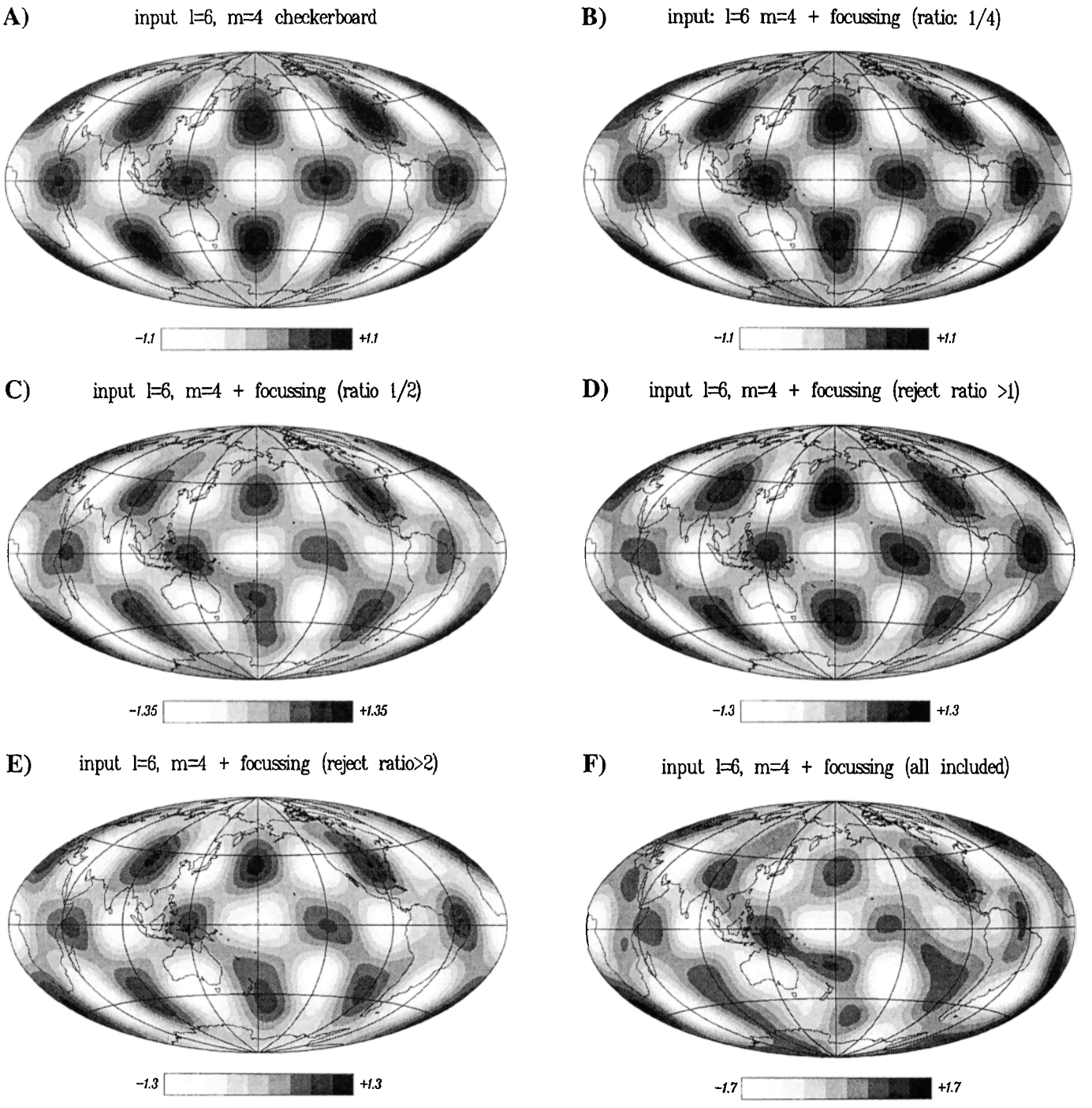

Figure 13. Results of a synthetic experiment in which we start with a checkerboard model of lateral variations in Q, as shown in (a), and compute amplitude anomalies on paths corresponding to our actual data set by adding focussing effects corresponding to the 3D elastic model of *Montagner and Tanimoto* [1992]. We then invert the resulting data set, assuming all amplitude anomalies are due to Q, keeping paths corresponding to different ratios f of focussing/attenuation anomalies: (b) f=0.25, (c) f=0.5, (d) f=1, (e) f=2., and (f) all data, including paths for which the ratio f is greater than 10.

Acknowledgments. The author is indebted to Shingo Watada for performing the variational calculations used in the synthetic tests in this paper. She also thanks Joe Durek and Goran Ekstrom for making their manuscripts available to her prior to publication. This manuscript benefitted from valuable discussions with Joe Durek and Jean-Paul Montagner. This research was supported by NSF-EAR grant 9204631. U.C. Berkeley Seismographic Station contribution 95-05.

References

Anderson, D. L., A. Ben-Menahem and C. B. Archambeau, Attenuation of seismic energy in the upper mantle, *J. Geophys. Res., 70*, 1441-1448, 1965.

Bussy, M., J.P. Montagner and B. Romanowicz, Tomographic study of upper mantle attenuation in the Pacific Ocean, *Geophys. Res. Lett, 20*, 663-666, 1993.

Calmant, S., and A. Cazenave, Anomalous elastic thickness of the oceanic lithosphere in the south-central Pacific, *Nature, 328*, 236-238, 1987.

Canas, J. A. and B. J. Mitchell, Lateral variation of surface wave anelastic attenuation across the Pacific, *Bull. Seism. Soc. Am., 68*, 1637-1650, 1978.

Chan, W. W. and Z. A. Der, Attenuation of multiple ScS in various parts of the world, *Geophys. J. 92*, 303-314, 1988.

Chapman D. S., Continental heat flow , in *Landolt-Bornstein Numerical Data and Functional Relationships in Science and Technology*, new series vol. 2, pp. 1-19, edited by K. Fuchs and H. Soffel , Springer-Verlag, 1985.

Davies G. F., Ocean bathymetry and mantle convection 1. Large scale flow and hotspots, *J. Geophys. Res., 93*, 10,467-10,480, 1988.

Davies G. F. , Mantle plumes, mantle stirring and hotspot geochemistry, *Earth Planet. Sci. Lett., 99*, 94-109, 1990.

Ding, C.-Y., and S. P. Grand, Upper Mantle Q structure beneath the East pacific Rise, *J. Geophys. Res., 98*, 1973-1985, 1993.

Deschamps, A., Inversion of the attenuation data of free oscillations of the Earth (fundamental and first higher modes), *Geophys. J. R. astr. Soc.*, , 50, 699-722, 1977.

Durek, J.J. and G. Ekstrom, A model of radial anelasticiy consistent with observed surface wave attenuation, *Bull. Seism. Soc. Am., in press*, 1994.

Durek, J. J. , M. H. Ritzwoller and J. H. Woodhouse, Constraining upper mantle anelasticity using surface wave amplitudes, *Geophys. J. Int., 114*, 249-272, 1993.

Dziewonski, A. M., and D. L. Anderson, Preliminary reference earth model, *Phys. Earth Planet. Inter., 25*, 297-356, 1981.

Dziewonski, A., and J. Steim, Dispersion and attenuation of mantle waves through waveform inversion, *Geophys. J. R. astron. Soc., 70*, 503-527, 1983.

Dziewonski, A. M., G. Chou, and J. H. Woodhouse, Determination of earthquake source parameters from waveform modelling, *J. Geophys. Res., 86*, 2825-2852, 1981.

Flanagan, M. P., and D. A. Wiens, Attenuation structure beneath the Lau back arc spreading center from teleseismic S phases, *Geophys. Res. Lett., 17*, 2117-2120, 1990.

Forte, A. M., R. L. Woodward and A. M. Dziewonski, Joint inversions of seismic and geodynamic data for models of three-dimensional mantle heterogeneity, *J. Geophys. Res., 99*, 21,857-21,877, 1994.

Gurnis, M., and S. Zhong, Generation of long wavelength heterogeneity in the mantle by the dynamic interaction between plates and convection, *Geophys. Res. Lett., 18*, 581-584, 1991.

Hager, B., R. W. Clayton, M. A. Richards, R. P. Comer and A. M. Dziewonski, Lower mantle heterogeneity, dynamic topography and the geoid, *Nature, 313*, 541-545, 1985.

Hansen, U., D. A. Yuen, S. E. Kroening and T. B. Larsen, Dynamical consequences of depth-dependent thermal expansivity and viscosity on mantle circulations and thermal structure, *Phys. Earth. Planet. Int., 77*, 205-223, 1993.

Jackson I., M. S. Paterson, and J. D. FitzGerald, Seismic wave dispersion and attenuation in Aheim dunite: an experimental study, *Geophys. J. Int. 108*, 517-534, 1992.

Jobert, N., and G. Roult, Periods and damping of free oscillations observed in France after sixteen earthquakes, *Geophys.J. R. astron. Soc., 45*, 155-176, 1978.

Jordan T. H., Global tectonic regionalization for seismological data analysis, *Bull. Seismol. Soc. Am., 71*, 1131-1141, 1981.

Kampfmann, W., and H. Berckhemer, High temperature experiments on the elastic and anelastic behaviour of magmatic rocks, *Phys. Earth. Planet. Inter. 40*, 223-247, 1985.

Karato, S.-I., Importance of anelasticity in the interpretation of seismic tomography, *Geophys. Res. Lett., 20*, 1623-1626, 1993.

Kellogg, L. H. and G. J. Wasserburg, The role of plumes in mantle helium fluxes, *Earth. Planet. Sci. Lett., 99*, 276-289, 1990.

King, S., and T. G. Masters, An inversion for the radial viscosity structure using seismic tomography, *Geophys. Res. Lett., 19*, 1551-1554, 1992.

Lay, T., and T. C. Wallace, Multiple ScS travel times and attenuation beneath Mexico and central America, *Geophys. Res. Lett., 10*, 301-304, 1983.

Lee, W. B. and S. C. Solomon, Simultaneous inversion of surface wave phase velocity and attenuation: Rayleigh and Love waves over continental and oceanic paths, *Bull. Seismol. Soc. Am., 69*, 65-95, 1979.

Liu, H. P., D. L. Anderson and H. Kanamori, Velcoity dispersion due to anelasticity: implication for seismology and mantle composition, *Geophys. J. R. astron. Soc., 47*, 41-58, 1976.

McNutt, M. K., and K. M. Fischer, The south Pacific superswell, in Seamounts, Islands and Atolls, *Geophys. Monogr. Ser., vol. 43*, edited by B. Keatinget al., AGU, Washington, D. C., 1987.

Mills, J., and A. Hales, Great circle Rayleigh wave attenuation and group velocity, part III, Inversion of global average group velocity and attenuation coefficients, *Phys. Earth Planet. Inter., 17*, 307-322, 1978.

Minster, J. B. and D. L. Anderson, A model of dislocation-controlled rheology for the mantle, *Philos. Trans. R. Soc. London, A, 299*, 319-356, 1981.

Mitchell, B. J., Regional Rayleigh wave attenuation in North America, *J. Geophys. Res., 80*, 4904-4916, 1975.

Mitchell, B. J., N. K. Yacoub, and A. M. Correig, A summary of seismic surface wave atteunation and its regional variation across continents and oceans, in *The earth's crust, Geophys. Monogr. Ser., vol 20*, edited by J. G. Heacock, pp 405-423, AGU, Washington, D. C., 1977.

Montagner, J. P., Regional three-dimensional structures using long-period surface waves, *Ann. Geophys., 4B3*, 283-294, 1986.

Montagner, J. P. and T. Tanimoto, Global anisotropy in the upper mantle inferred from the regionalization of phase velocities, *J. Geophys. Res., 95*, 4797-4819, 1991.

Montagner, J. P. and T. Tanimoto, Global upper mantle tomography of seismic velocities and anisotropies, *J. Geophys. Res., 96*, 20,337-20,351, 1992.

Montagner, J. P. and B. Romanowicz, Degrees 2-4-6 inferred from seismic tomography, *Geophys. Res. Lett., 20*, 631-634, 1993.

Nakanishi, I., Regional differences in the phase velocity and the quality factor Q of mantle Rayleigh waves, *Science, 200*, 1379-1381, 1978.

Nakanishi I., Attenuation of multiple ScS waves beneath the Japanese Arc,*Phys. Earth Planet. Inter., 19*, 337-347, 1979.

Park, J., Asymptotic coulped mode expressions for multiplet amplitude anomalies and frequency shifts on an aspherical earth, *Geophys. J. R. astr. Soc., 90*, 129-164, 1987.

Resovsky, J. S. and M. H. Ritzwoller, Characterizing long-period seismic effects of long-wavelength elastic and anelastic models, *Geophys. J. Int., 117*, 365-393, 1994.

Revenaugh, J. S. and T. H. Jordan, A study of mantle layering beneath the western Pacific, *J. Geophys. Res., 94, 5787-5813*, 1989.

Ricard, Y., M. Richards, C. Lithgow-Bertelloni, and Y. LeStunff, A geodynamic model of mantle density heterogeneity, *J. Geophys. Res., 89*, 5987-6002, 1993.

Richards M. A., B. H. Hager, and N. H. Sleep, Dynamically supported geoid highs over hotspots: observation and theory, *J. Geophys. Res, 93*, 7690-7708, 1988.

Romanowicz, B., Multiplet-multiplet coupling due to lateral heterogeneity: asymptotic effects on the amplitude and frequency of the Earth's normal modes, *Geophys. J. R. astron. Soc., 90*, 75-100, 1987.

Romanowicz, B., The upper mantle degree 2: constraints and inferences from global mantle wave attenuation measurements, *J. Geophys. Res., 95*, 11,051-11,071, 1990.

Romanowicz, B., On the measurement of anelastic attenuation using amplitudes of low frequency surface waves,*Phys. Earth Planet. Inter., 84*, 179-191, 1994a.

Romanowicz, B., Anelastic tomography: a new perspective on upper-mantle thermal structure, *Earth. Planet. Sci. Lett., 128*, 113-121, 1994b.

Romanowicz, B., G. Roult, and T. Kohl, The upper mantle degree two pattern: constraints from Geoscope fundamental spheroidal model eigenfrequency and attenuation measurements, *Geophys. Res. Lett., 14*, 1219-1222, 1987.

Romanowicz, B., et al., The Geoscope program: present status and perspectives, *Bull. Seismol. Soc. Am., 81*, 243-264, 1991.

Roult, G., The effect of young oceanic regions on the periods and damping of free oscillations of the earth, *J. Geophys., 51, 38-43*, 1982.

Roult, G., B. Romanowicz and J. P. Montagner, 3D upper mantle shear velocity and attenuation from fundamental mode free oscillation data, *Geophys. J. Int., 101, 61-80*, 1990.

Sailor, R. V., and A. M. Dziewonski, Measurements and interpretation of normal mode attenuation, *Geophys. J. R. astron . Soc., 53*, 559-581, 1978.

Sheehan, A. F., and S. C. Solomon, Differential shear wave attenuation and its lateral variation in the north Atlantic region, *J. Geophys. Res., 97*, 15,339-15,350, 1992.

Sipkin, S. A. and T. H. Jordan, Frequency dependence of QScS, *Bull. Seismol. Soc. Am., 69*, 1055-1079, 1979.

Sipkin S. A. and T. H. Jordan, Regional variations of Q_{ScS}, *Bull. Seismol. Soc. Am., 70*, 1071-1102, 1980.

Sleep N., Hotspots and mantle plumes: some phenomenology, *J. Geophys. Res., 95*, 6715-6736, 1990.

Smith, M. F., and G. Masters, Aspherical structure constraints from free oscillation frequency and attenuation measurements, *J. Geophys. Res., 94*, 1953-1976, 1989.

Solheim, L. P., and W. R. Peltier, Phase boundary deflections at 660-km depth and episodically layered isochemical convection in the mantle, *J. Geophys. Res., 99*, 15,861-15,875, 1994.

Su, W. J., R. Woodward, and A. M. Dziewonski, Degree 12 model of shear velocity heterogeneity in the mantle, *J. Geophys. Res., 99*, 6945-6980, 1994.

Suda, N., N. Shibata, and Y. Fukao, Degree-2 pattern of attenuation structure in the upper mantle from apparent complex frequency measurements of fundamental spheroidal modes, *Geophys. Res. Lett., 18*, 1119-1122, 1991.

Tackley P., D. J. Stevenson, G. A. Glazmaier, and G. Schubert, Effects of an endothermic phase transition at 670 km depth in a spherical model of convection in th Earth's mantle, *Nature 361*, 699-704, 1993.

Tanimoto, T., The Backus-Gilbert approach to the 3-D structure in the upper mantle, II, SH and SV velocity, *Geophys. J. R. Astron. Soc., 84*, 49-69, 1986.

Tarantola, A. and B. Valette, Generalized nonlinear inverse problems solved using the least squares criterion, *Rev. Geophys., 20*, 219-232, 1982.

Widmer, R. , G. Masters, and F. Gilbert, Spherically symmetric attenuation within the earth from normal mode data, *Geophys. J. Int., 104*, 541-553., 1991.

White W. M. , Sources of oceanic basalts: radiogenic isotope evidence, *Geology, 13*, 115-118, 1985.

Woodhouse, J. H., and A. M. Dziewonski, Mapping the upper mantle: three-dimensional modeling of the earth structure by inversion of seismic waveforms, *J. Geophys. Res., 89*, 5953-5986, 1984.

Woodhouse, J. H., and Y. Wong, Amplitude, phase and path anomalies of mantle waves, *Geophys. J. R. Astron. Soc., 87*, 753-773, 1986.

Yacoub N. K., and B. J. Mitchell, Attenuation of Rayleigh wave amplitudes across Eurasia, *Bull. Seism. Soc. Am. 67*, 751-769, 1977.

Zhang, Y. S. and T. Tanimoto, High-reslution global upper mantle structure and plate tectonics, *J. Geophys. Res., 98*, 9793-9823, 1993.

Barbara Romanowicz, Seismographic Station, 475 McCone Hall, Berkeley, CA 94720. (e-mail: barbara@seismo.berkeley.edu)

(Received September 26, 1994; revised March 14, 1995; accepted March 20, 1995.)